Research Article
Journal of Geophysical Research: Oceans
DOI 10.1002/2016JC012668

Influence of the phytoplankton community structure on the spring and annual primary production in the North-Western Mediterranean Sea

Nicolas Mayot[1], Fabrizio D'Ortenzio[1], Julia Uitz[1], Bernard Gentili[1], Joséphine Ras[1], Vincenzo Vellucci[1], Melek Golbol[1], David Antoine[1,2] and Hervé Claustre[1]

[1]Sorbonne Universités, UPMC Univ Paris 06, INSU-CNRS, Laboratoire d'Océanographie de Villefranche (LOV), 181 Chemin du Lazaret, 06230 Villefranche-sur-mer, France.

[2]Remote Sensing and Satellite Research Group, Department of Physics and Astronomy, Curtin University, Perth, Western Australia 6845, Australia

Key Words: phytoplankton community structure; primary production; spring bloom; inter-annual variability

Key Points:

- Diatoms' contributions to biomass and primary production during the spring bloom are enhanced by intense winter deep convection
- The springtime shift in phytoplankton community structure that is induced by deep convection could affect the biological carbon pump

Received: Dec 28, 2016; Revised: Mar 14, 2017; Accepted: Mar 14, 2017

Abstract: Satellite ocean color observations revealed that unusually deep convection events in 2005, 2006, 2010 and 2013 led to an increased phytoplankton biomass during the spring bloom over a large area of the North-Western Mediterranean Sea (NWM). Here we investigate the effects of these events on the seasonal phytoplankton community structure, we quantify their influence on primary production, and we discuss the potential biogeochemical impact. For this purpose, we compiled *in situ* phytoplankton pigment data from five ship surveys performed in the NWM and from monthly cruises at a fixed station in the Ligurian Sea. We derived primary production rates from a light-photosynthesis model applied to these *in situ* data. Our results confirm that the maximum phytoplankton biomass during the spring bloom is larger in years associated with intense deep convection events (+ 51%). During these enhanced spring blooms, the contribution of diatoms to total phytoplankton biomass increased (+ 33 %), as well as the primary production rate (+ 115 %). The occurrence of a highly productive bloom is also related to an increase in the phytoplankton bloom area (+ 155 %), and in the relative contribution of diatoms to primary production (+ 63 %). Therefore, assuming that deep convection in the NWM could be significantly weakened by future climate changes, substantial decreases in the spring production of organic carbon and of its export to deep waters can be expected.

1 Introduction

The size and taxonomic structure of phytoplankton communities regulate the functioning of marine ecosystems and biogeochemical cycles (e.g. [*Legendre and Le Fèvre*, 1991; *Quere et al.*, 2005; *Hood et al.*, 2006]). For example, the photosynthetic efficiency of phytoplankton communities is generally affected by their size structure [*Bouman et al.*, 2005; *Uitz et al.*, 2008; *Brewin et al.*, 2010; *Edwards et al.*, 2015], with potential impact on the export of particulate organic carbon (POC) to the deep oceans [*Boyd and Newton*, 1999]. Pico-phytoplankton (< 2 μm) are generally associated with slow sinking rates and microbial loop systems [*Legendre and Le Fèvre*, 1991; *Michaels et al.*, 1994], although they can contribute significantly to the carbon export to depth through eddy-driven subduction processes [*Omand et al.*, 2015] or following the increase of their sinking speed and rate of consumption by zooplankton through aggregation mechanisms [*Richardson and Jackson*, 2007]. Conversely, large phytoplankton, such as diatoms, typically produce large and rapidly-sinking materials. Indeed, an increase in the contribution of micro-phytoplankton (mainly diatoms) to the total phytoplankton biomass has been observed to correlate with the rate of POC exported to depth [*Guidi et al.*, 2009, 2015; *Henson et al.*, 2012], with significant consequences on the amount of POC potentially sequestered in the deep oceans, i.e., the so-called biological carbon pump.

The North-Western Mediterranean Sea (NWM) displays the characteristics of a typical temperate oceanic region, with a pronounced spring phytoplankton bloom in shallow mixed layers. For this reason, and despite its relatively limited surface area, the NWM is a key region to study phytoplankton bloom dynamics [*Mermex Group*, 2011]. When the NWM spring bloom initiates, the micro-phytoplankton biomass, mainly composed of diatoms, rapidly increases and reaches an annual maximum generally in March [*Marty et al.*, 2002; *Siokou-Frangou et al.*, 2010; *Estrada and Vaqué*, 2014]. Then, the development of a surface nano-phytoplankton biomass maximum can be observed [*Marty et al.*, 2002; *Siokou-Frangou et al.*, 2010; *Estrada and Vaqué*, 2014], which precedes the end of the spring bloom and the establishment of a summer phytoplankton community dominated by nano- and pico-phytoplankton [*Marty et al.*, 2002; *Siokou-Frangou et al.*, 2010; *Estrada and Vaqué*, 2014].

The NWM is also one of the most productive regions of the Mediterranean Sea with annual primary production values ranging between 86 and 232 gC m^{-2} (estimates based on *in situ* measurements [*Marty and Chiavérini*, 2002]). These values are significantly higher than in the Eastern Mediterranean basin which is characterized by subtropical-like values (20.3-61.8 gC m^{-2}, estimates based on *in situ* measurements [*Siokou-Frangou et al.*, 2010]). Estimates of annual primary production in the NWM derived from bio-optical primary production models applied to satellite ocean color data fall within the same range of values (78-204 gC m^{-2}, *Morel and André*, 1991; *Antoine et al.*, 1995; *Bosc et al.*, 2004; *Olita et al.*, 2011a; *Uitz et al.*, 2012]).

Nano-phytoplankton contribute the largest part of the annual primary production in the NWM, although micro-phytoplankton (mainly diatoms) significantly support spring production [*Marty and Chiavérini*, 2002; *Uitz et al.*, 2012]. The occurrence of diatoms, although relatively limited in time, is critical for the export of POC to depth [*Heussner et al.*, 2006; *Miquel et al.*, 2011; *Stabholz et al.*, 2013; *Ramondenc et al.*, 2016]. The amount of POC exported at depth in the NWM is then particularly high compared to the rest of the Mediterranean basin, which is mostly dominated by a microbial-loop activity [*Siokou-Frangou et al.*, 2010; *Estrada and Vaqué*, 2014].

Atmospheric conditions over the NWM during specific years induce particularly cold and windy winters and, consequently, deep convection events [*MEDOC Group*, 1970; *Millot*, 1999; *Houpert et al.*, submit]. It has also been observed that these extreme atmospheric conditions and deep winter mixed layers are followed by elevated spring chlorophyll-*a* concentrations ([Chl-a], proxy of the phytoplankton biomass) [*San Feliu and Muñoz*, 1971; *Estrada*, 1996; *Marty et al.*, 2002; *Marty and Chiavérini*, 2010; *Arin et al.*, 2013; *Estrada et al.*, 2014; *Severin et al.*, 2014]. Spring diatom biomass and the subsequent diatom valve flux at depth have also been found to be greater than average after the occurrence of deep winter mixing events [*Rigual-Hernández et al.*, 2013]. Additional studies based on satellite data have reported an increase in surface [Chl-a] after particularly cold and windy winters, and suggested also that a high spring phytoplankton biomass may be related to the expansion of the phytoplankton blooming area [*Olita et al.*, 2011b; *Volpe et al.*, 2012; *Lavigne et al.*, 2013; *Mayot et al.*, 2016]. Regional 3D models applied to the NWM [*Herrmann et al.*, 2013; *Auger et al.*, 2014; *Ulses et al.*, 2016] have also demonstrated strong inter-annual variability in the spring primary production related to the depth of winter mixed layers. Therefore, the alternation of mild winters (shallow mixed layers) and colder winters (deep mixed layers) presumably modulates spring phytoplankton biomass accumulation and production in the NWM.

Previous results are, however, either sparse or intermittent (when derived from *in situ* data), or limited to the surface layer of the ocean (satellite data), or of theoretical nature when derived from model simulations. Thus the influence of the depth of the winter mixed layers on the spring phytoplankton biomass and community structure still needs to be confirmed with *in situ* data relevant to the scale of the NWM sub-basin. In addition, the consequence of changes in the spring phytoplankton biomass and community structure on the seasonal and annual primary production yet remains to be investigated. This would provide valuable information on the stock of organic carbon associated with each phytoplankton size class in the NWM, which could in turn be potentially correlated with the amount of POC exported to depth in this basin. These investigations are crucial for the possible impact of climate change on the

biological carbon pump to be assessed in the NWM, where a shift towards warmer and drier conditions has been predicted [*IPCC*, 2013; *Mariotti et al.*, 2015].

To derive robust cause-effect relationships between the depths of winter mixed layers and the spring phytoplankton dynamics (i.e. biomass and community structure) when using in situ observations, a specific and dedicated effort in data analysis is required. Here, a spatial division of the Mediterranean Sea into ecological units, referred to as trophic regimes, has been used [*Mayot et al.*, 2016]. These trophic regimes have been determined through a cluster analysis of the seasonal cycles of satellite-derived surface [Chl-a]. According to the main hypothesis, the similarity of the seasonal cycle of surface [Chl-a] should reflect similar environmental forcing (physical and biogeochemical), although the criteria used to determine the trophic regimes still need to be improved. The *in situ* observations performed at different times in a given trophic regime were then pooled together, with the aim of reconstructing as complete as possible annual time series of *in situ* observations for each trophic regime observed in the NWM.

In the description by [*Mayot et al.*, 2016], the NWM is mainly characterized by a trophic regime with a seasonal cycle of [Chl-a] displaying a spring bloom, i.e. the "Bloom" trophic regime [*Mayot et al.*, 2016]. During years associated with extreme winter atmospheric conditions and very deep winter mixed layers, the "Bloom" trophic regime is partially replaced by another trophic regime, characterized by a similar seasonal cycle of [Chl-a] but with an enhanced and delayed spring bloom. The latter is referred to as the "High Bloom" trophic regime [*Mayot et al.*, 2016].

These two trophic regimes are used here as a framework to examine the inter-annual variability of primary production in the NWM. They represent two contrasting situations that occur in the NWM: the "Bloom" trophic regime reflects the average situation, while the "High Bloom" trophic regime depicts the occasional situation of an enhanced spring phytoplankton bloom following very deep winter mixed layers. We investigate the differences in the phytoplankton community structure, as well as in the seasonal and annual primary production that exist between these two trophic regimes. Our threefold objective is: (1) to investigate, using *in situ* observations, the effects of the different winter mixing conditions associated with the "Bloom" and "High Bloom" trophic regimes on the seasonal phytoplankton community composition (described on the basis of the size structure); (2) to quantify, using a light-photosynthesis model, how changes in the phytoplankton community structure, induced by changes in winter mixing conditions, influence the seasonal and annual primary production rates; and (3) to discuss the potential biogeochemical impact of intermittence between Bloom *vs.* High Bloom conditions in the context of future climate change. The *in situ* observations comprise vertical distribution of phytoplankton pigments, converted into vertical distribution of biomass associated with three phytoplankton size classes [*Uitz et al.,* 2006]. The light-photosynthesis model accounts for the size-structure of the phytoplankton community [*Morel*, 1991; *Uitz et al.*, 2008]. The analysis is conducted with pigment data collected over the whole NWM at each season between July 2012 and July 2013 (the two trophic regimes were present during this period), and also with pigment data from a multiannual open-ocean time-series in a sub-basin of the NWM (*i.e.* in the Ligurian Sea) affected by the inter-annual presence of the two trophic regimes.

2 Data and Methods

2.1 Studied area and sampling plan

The NWM presents a large scale cyclonic circulation (Figure 1), confined on the North-western boundary by the Northern Current that flows southwards along the coasts, by the permanent thermal Balearic Front at the South, and by the Western Corsica Current [*Millot*, 1999]. In winter, under the influence of atmospheric and hydrological forcing, the central zone of the cyclonic circulation, located south of the Gulf of Lion, may be subject to deep convection events that induce the formation of deep waters [*MEDOC Group*, 1970; *Millot*, 1999].

In the NWM an intensive sampling effort was carried out between July 2012 and July 2013, with five ship surveys on board R/V *Le Suroît* and R/V *Tethys II* (DEep Water Experiment, DEWEX [*Testor et al.*, submitted], coupled with the Mediterranean Ocean Observing System for the Environment, MOOSE, http://www.moose-network.fr/, Table 1). The DEWEX ship surveys were coupled with *in situ* observations from 13 Argo floats, four BGC-Argo floats and 10 Bio-optical gliders (Table 1).

Here *in situ* observations collected monthly in the Ligurian Sea in the framework of the long-term DYFAMED (Dynamics of Atmospheric Fluxes in the Mediterranean Sea) and BOUSSOLE (Buoy for the acquisition of a Long-Term Optical Time Series) programs (site located 43°22' N, 7°54'E, Table 1) have also been used.

2.2 Measured variables

We selected the deep (bathymetry > 1000 m) offshore stations of the five DEWEX ship surveys (Figure 1), and performed by the autonomous platforms (i.e. Bio-optical gliders, and Argo and BGC-Argo floats), for which conductivity-temperature-depth (CTD) and, occasionally, chlorophyll-*a* fluorescence sensors were available (see Table 1). For the monthly cruises at the DYFAMED/BOUSSOLE site, a CTD is systematically deployed in conjunction with a chlorophyll-*a* fluorometer (except before 2004 at the DYFAMED sampling site, in total 231 stations performed, Table 1). Quality control procedures on the selected temperature, salinity and fluorescence profiles (when available) are detailed in *Mayot et al.* [submitted]. The temperature and salinity profiles were used to determine the potential density profile. The mixed layer depth (MLD) was then derived from the density profile, by using the 0.01 kg m^{-3} criterion with the density at 10 m as a reference [*Mayot et al.*, submitted].

The vertical distribution of phytoplankton pigment concentrations was determined through discrete water samples collected at 12 depths along the water column with Niskin bottles mounted on the CTD rosette. The discrete water samples were then filtered (GF/F) and High-Performance Liquid Chromatography (HPLC) analyses were performed to determine the concentration of the different phytoplankton pigments present in these water samples. All HPLC measurements used here were conducted at the *Laboratoire d'Océanographie de Villefranche* (see [*Ras et al.*, 2008] for details on the HPLC method). Sampling for subsequent phytoplankton pigment analyses is systematically performed during the monthly cruises at the DYFAMED/BOUSSOLE site and was also carried out during four DEWEX cruises (between 10 and 17 stations per cruise, Table 1).

2.3 Determination of the phytoplankton community structure

Chlorophyll-*a*, here refers to the sum of (monovinyl) chlorophyll-*a*, divinyl chlorophyll-*a*, chlorophyllide-a and the allomeric and epimeric forms of chlorophyll-a, is ubiquitous to all phytoplankton cells (note that prochlorophytes contain only the divinyl chlorophyll-a). The [Chl-a] is used here as a proxy of phytoplankton biomass. In contrast to chlorophyll-*a*, the composition of accessory pigments varies among phytoplankton groups. Some of them are specific biomarkers of certain phytoplankton taxa and may be used to estimate the structure of phytoplankton communities. Here we followed the approach proposed by *Claustre*, [1994] and further modified by *Vidussi et al.* [2001] and *Uitz et al.* [2006]. Briefly, seven diagnostic pigments were selected as biomarkers of major phytoplankton taxa: fucoxanthin (Fuco), peridinin (Perid), alloxanthin (Allo), 19'-butanoyloxyfucoxanthin (ButFuco), 19'-hexanoyloxyfucoxanthin (HexFuco), zeaxanthin (Zea) and total chlorophyll-*b* (chlorophyll-*b* + divinyl chlorophyll-*b*, TChlb). These seven diagnostic pigments were then assigned to either of the pico-, nano- or micro-phytoplankton size classes, depending on the typical cell size of the phytoplankton organisms within each taxon. The taxonomic and size correspondence of each diagnostic pigment is presented in Table 2.

The diagnostic pigment-based approach can be further used to estimate the relative contribution of the three size classes to the [Chl-a] associated with the total algal biomass, f_{micro}, f_{nano} and f_{pico},

$$f_{\mathrm{micro}} = (1.41[\mathrm{Fuco}] + 1.41[\mathrm{Perid}])/\sum \mathrm{DPW} \quad (1a)$$

$$f_{\mathrm{nano}} = (1.27[\mathrm{HexFuco}] + 0.35[\mathrm{ButFuco}] + 0.60[\mathrm{Allo}])/\sum \mathrm{DPW} \quad (1b)$$

$$f_{\mathrm{pico}} = (1.01[\mathrm{TChlb}] + 0.86[\mathrm{Zea}])/\sum \mathrm{DPW} \quad (1c)$$

with $\sum$DPW the sum of the weighted concentrations of the seven diagnostic pigments :

$$\sum \mathrm{DPW} = (1.41[\mathrm{Fuco}] + 1.41[\mathrm{Perid}] + 1.27[\mathrm{HexFuco}] + 0.35[\mathrm{ButFuco}] + 0.60[\mathrm{Allo}] + 1.01[\mathrm{TChlb}] + 0.86[\mathrm{Zea}]) \quad (2)$$

In equations (1) and (2), the coefficients represent an average ratio between the concentration of each diagnostic pigment and [Chl-a], and were obtained from a multiple regression analysis applied to a global pigment dataset [*Uitz et al.*, 2006]. Then, equations (1a,b,c) were applied at all depths (z) of all vertical profiles of phytoplankton pigment concentrations performed during the DEWEX cruises and at the DYFAMED/BOUSSOLE site in order to obtain vertical profiles of [Chl-a] associated with the three phytoplankton size classes:

$$[\mathrm{Chl-a}]_{\mathrm{micro}}(z) = [\mathrm{Chl-a}](\mathrm{z}) \times f_{\mathrm{micro}}(z) \quad (3a)$$

$$[\mathrm{Chl-a}]_{\mathrm{nano}}(z) = [\mathrm{Chl-a}](\mathrm{z}) \times f_{\mathrm{nano}}(z) \quad (3b)$$

$$[\mathrm{Chl-a}]_{\mathrm{pico}}(z) = [\mathrm{Chl-a}](\mathrm{z}) \times f_{\mathrm{pico}}(z) \quad (3c)$$

The seasonal variation of the class-specific [Chl-a] (associated with the three phytoplankton size classes pico-, nano- and micro-phytoplankton) were integrated from the surface down to 1.5 times the euphotic depth ($[\mathrm{Chl\text{-}a}]_{1.5*Zeu}$), inasmuch a significant phytoplankton biomass can often be observed below the euphotic depth [*Morel and Berthon*, 1989]. For this purpose, the vertical profiles of the [Chl-a] (i.e. [Chl-a](z)) were used to determine the euphotic depth [*Morel and Berthon*, 1989; *Morel and Maritorena*, 2001]. The seasonal variation of the total

$[Chl\text{-}a]_{1.5*Zeu}$ was also obtained from fluorometers calibrated with HPLC data (the calibration is fully presented in [*Mayot et al.,* submitted]). But for the fluorometers measurements, the euphotic depth was derived from ocean color images of surface [Chl-a] [*Morel et al.*, 2007].

2.4 Coupling *in situ* observations with trophic regimes

The HPLC-derived pigment data available for this work are numerous yet still scarce at the scale of the NWM. Therefore, they were pooled together to construct pertinent annual cycles of $[Chl\text{-}a]_{1.5*Zeu}$ and other variables. The approach is based on a spatial division of the Mediterranean Sea from satellite ocean color images of surface [Chl-a] [*Mayot et al.*, 2016], which allows identifying two main trophic regimes in the NWM, called "Bloom" and "High Bloom" (Figure 2).

For the DEWEX cruises and the autonomous platforms deployed between July 2012 and July 2013, each individual profile was classified as "Bloom" or "High Bloom" by matching its location with that of the trophic regimes in the NWM for the year 2012/13 (Figure 1). All *in situ* observations related to a given trophic regime were pooled together and sorted in chronological order, thus producing a time-series associated with each trophic regime.

Following the same logic, the in situ observations available at the DYFAMED/BOUSSOLE site between 1998 and 2014 have to be also classified as "Bloom" or "High Bloom". For this, 75 % of the surface of an area 36 km in diameter around the DYFAMED/BOUSSOLE site – that is, 16 satellite pixels of 9 km² – must be classified as "Bloom" or "High Bloom". Therefore, the in situ observations available at the DYFAMED/BOUSSOLE site between 1998 and 2014 were labeled "High Bloom" for 1999/00, 2002/03, 2006/07, 2009/10, 2011/12 and 2012/13, "Bloom" for 1998/99, 2004/05, 2005/06 and 2007/08, and discarded when the region was a mixed between them or not classified (i.e. white areas on Figure 2). Once the *in situ* data had been classified, they were pooled together to reconstruct a climatological time-series of *in situ* observations for each trophic regime at an 8-day resolution (data collected the same 8-day week were pooled together, a mean value was calculated and the remaining gaps in the time series were filled using linear interpolation).

The data processing resulted in a time-series of *in situ* observations for each trophic regime during the DEWEX study period (2012/13) and at the DYFAMED/BOUSSOLE site. The two were also merged into a climatological time series for each trophic regime ("merged time-series"), subsequently used to compute primary production.

2.5 Estimation of total and class-specific primary production

Phytoplankton primary production was estimated using a light-photosynthesis model applied to the climatological merged time series of *in situ* [Chl-a] vertical profiles obtained by merging the DYFAMED/BOUSSLE and DEWEX data sets. Equations (3a,b,c) provided the fractional contribution of the three phytoplankton size classes (pico-, nano- and micro-phytoplankton) to all *in situ* [Chl-a] profiles. Using these profiles, the *Morel* [1991] light-photosynthesis model, combined with the *Uitz et al.* [2008] phytoplankton class-specific photophysiological properties, provided an estimate of the primary production associated with each of the three phytoplankton size classes (P_{micro}, P_{nano} and P_{pico}) that were then summed up to produce the total phytoplankton production (P_{tot}). More details of the light-photosynthesis model used here can be found in the supporting information [*Platt et al.*, 1980; *Lewis et al.*, 1985; *Morel*, 1988; *Uitz et al.*, 2008]. The required daily surface Photosynthetically Available

Radiation (PAR) was retrieved from the GlobColour merged ocean color satellite product (spatial resolution of 4 km, http://www.globcolour.info).

3 Results

3.1 Seasonal cycle of phytoplankton chlorophyll and community structure, and of the MLD

Over July 2012 to July 2013 (DEWEX cruises) the seasonal variation of $[Chl\text{-}a]_{1.5*Zeu}$ measured with fluorometers is similar for the "Bloom" and "High Bloom" trophic regimes (Figure 3a-b). Low values are observed in winter (December, January, February), followed by a maximal annual value in spring (March, April, May), with intermediate values during summer (June, July, August) and autumn (September, October, November). The spring maximal value is higher in the "High Bloom" trophic regime (171 mg m^{-2}) than in the "Bloom" trophic regime (90 mg m^{-2}). Available HPLC measurements of $[Chl\text{-}a]_{1.5*Zeu}$ (grey points in Figure 3a-b) confirm the seasonal variations of the $[Chl\text{-}a]_{1.5*Zeu}$ measured with the fluorometers.

Overall, and for both trophic regimes, the proportion of micro-phytoplankton is low in autumn and summer, increases in winter, and reaches maximal values in spring (Figure 3c-d). Pico-phytoplankton is present in high proportions in autumn, decreases in winter, and reaches very low values in spring and summer. Finally, the proportion of nano-phytoplankton is very high in summer and low in autumn, winter and spring. The seasonal cycles associated with the two trophic regimes are also illustrated in the ternary plot (Figure 4), with the proportion of micro-phytoplankton increasing from low values in summer (< 25%) to a maximum in spring (> 40%). For both trophic regimes, the proportions of nano- and pico-phytoplankton are low in spring and high in summer (> 70 %) and autumn (> 40 %) respectively.

Different patterns can be distinguished between the two trophic regimes when comparing the phytoplankton community structures in winter and spring (Figure 4). In the "Bloom" trophic regime, the proportion of nano-phytoplankton in winter is higher (around 40 %) than that of micro- and pico-phytoplankton (both around 30 %). For the "High Bloom" trophic regime, the proportions of nano- and micro-phytoplankton vary similarly in winter (each around 40 %) while pico-phytoplankton are in lower proportions (around 25 %). In spring, the proportion of nano-phytoplankton still is the highest in the "Bloom" trophic regime (values mainly around 40-60 %) with the proportion of micro-phytoplankton that rarely exceeded 40 %. In the "High Bloom" trophic regime, micro-phytoplankton commonly exceeded 40 % (most of the values around 50 %).

For both trophic regimes, the annual cycle of the MLD presents a summer/spring minimum and a winter maximum (Figure 3e-f). However, the wintertime MLD is deeper in the "High Bloom" trophic regime (two mean MLD maxima > 880 m) than in the "Bloom" trophic regime (a mean MLD maximum ~475 m). The BGC-Argo floats and the bio-optical gliders did not sample deeper than 1000 m, while the maximum depth of Argo floats is 2000 m and the ship-based CTD casts were done throughout the water column. Therefore, 1000 m represents the highest possible MLD value in the Figure 3e-f, although in this figure dark points indicate the estimations higher than or equal to 2000 m (i.e. from Argo floats and ship-based profiles). The number of very deep MLD estimations (MLD ≥ 2000 m) during winter is larger in the "High Bloom" trophic regime (16) than in the "Bloom" trophic regime (1).

The climatological time-series of $[Chl\text{-}a]_{1.5*Zeu}$ calculated at the DYFAMED/BOUSSOLE site and for the two trophic regimes (Figure 5a-b) indicates a higher spring maximal value for the "High Bloom" trophic regime (101 mg m^{-2}) than for the "Bloom" trophic regime (67 mg m^{-2}, Figure 5a-b). For the rest of the annual cycle, the observed values are relatively close for the two trophic regimes, ranging between 55 mg m^{-2} and 20 mg m^{-2}. As for the DEWEX cruises, the strongest differences in the phytoplankton community structure between the two trophic regimes can be observed in the springtime (Figure 5c-d, confirmed in the ternary plot of the Figure 6). During this season, the proportion of micro-phytoplankton is significantly higher in the "High Bloom" trophic regime (maximal value > 80 %), than for the "Bloom" trophic regime (maximal value < 65 %). Furthermore, for the "High Bloom" trophic regime, the spring proportion of nano-phytoplankton is lower (0-15 %) than for the "Bloom" trophic regime (mainly 20-30 %). The spring proportion of the pico-phytoplankton is similar for the two trophic regimes (10 %).

Climatological annual time series of MLD for the two trophic regimes were calculated from all CTD casts performed at the DYFAMED/BOUSSOLE site (Figure 5e-f). It must be emphasized that the values associated to these MLD time series deduced are underestimated since, (1) 400 m is the greatest depth of the CTD cast performed as part of the BOUSSOLE project, and (2) cruise sampling are cancelled in the case of adverse weather conditions (i.e., likely to generate very deep MLD). Despite these limitations, the wintertime MLD is deeper in the "High Bloom" trophic regime (a mean MLD maximum ~380 m) than in the "Bloom" trophic regime (a mean MLD maximum ~140 m).

To calculate the primary production of the two trophic regimes, the [Chl-a] profiles associated with the three phytoplankton size classes from the DEWEX cruises (Figure 3-4) and from the DYFAMED/BOUSSOLE site (Figure 5-6) were merged to obtain an annual climatological time-series of the biomass of each phytoplankton size class associated with the two studied trophic regimes (Figure 7a-d). As expected, the annual cycles of $[Chl\text{-}a]_{1.5*Zeu}$ (Figure 7a-b) are similar to the annual cycles already described (Figures 3a-b and 5a-b). At the beginning of the spring bloom, and for the two trophic regimes, the biomass of all phytoplankton size classes increases (Figure 7c-d). However the "Bloom" trophic regime displayed higher values (around 20 mg m^{-2} for the nano- and the micro-phytoplankton, and 15 mg m^{-2} for the pico-phytoplankton) than the "High Bloom" trophic regime (around 15 mg m^{-2} for the nano- and the micro-phytoplankton, and 8 mg m^{-2} for the pico-phytoplankton). In March both trophic regimes present a maximum of micro-phytoplankton biomass, followed in April by a nano-phytoplankton biomass maximum. The micro-phytoplankton peak is, however, different in timing and magnitude between the two trophic regimes, with later and higher values in the "High Bloom" trophic regime (late March and 60 mg m^{-2}) than in the "Bloom" trophic regime (mid-March and 40 mg m^{-2}). On the contrary, the nano-phytoplankton peaks are similar in magnitude and timing between the two trophic regimes (mid-April and around 30 mg m^{-2}). Similarly, all MLD estimations obtained from the DEWEX cruises (Figure 3e-f) and from the DYFAMED/BOUSSOLE site (Figure 5e-f) were merged to produce climatological time of MLD associated with the two trophic regimes. As anticipated, the "High Bloom" trophic regimes is associated with very deep MLD (a mean MLD maximum ~700 m, and numerous values higher than 2000 m), while the wintertime MLD is shallower in the "Bloom" trophic regime (a mean MLD maximum ~110 m).

3.2 Seasonal cycle of total and class-specific primary production

The climatological annual cycle of total primary production calculated for the "Bloom" and "High Bloom" trophic regimes (Figure 8a-b), with the DEWEX and DYFAMED/BOUSOLE merged data sets as input, both present a minimum in winter and a maximum in spring. The spring production period, i.e. when daily primary production exceeds 0.6 gC m^{-2} in winter and spring, is longer for the "Bloom" trophic regime (February to mid-May) than for the "High Bloom" trophic regime (March to mid-May). In addition, the maximum value of daily primary production in spring is lower for the "Bloom" trophic regime (1.1 gC m^{-2}) than for the "High Bloom" trophic regime (1.6 gC m^{-2}, + 45 %).

In both trophic regimes, the daily primary production (Figure 8c-d) is dominated by micro-phytoplankton (P_{micro}) in spring, and by nano-phytoplankton (P_{nano}) during the rest of the year. The daily primary production associated with pico-phytoplankton (P_{pico}) is generally low, except in autumn (September to November) when P_{pico} is higher than P_{micro}. The spring peak of P_{micro} is higher for the "High Bloom" trophic regime (0.8 gC m^{-2}) than for the "Bloom" trophic regime (0.4 gC m^{-2}). However, both trophic regimes display a similar spring peak of P_{nano} (0.55 gC m^{-2}, in mid-April).

The annually (July to July) integrated primary production rates are also similar for the two trophic regimes: 180 gC m^{-2} for the "Bloom" trophic regime and 191 gC m^{-2} for the "High Bloom" trophic regime (only 7 % difference, Figure 9a). A difference in the cumulated time series of primary production can, however, be observed in spring (Figure 9a). The spring period is mainly characterized by a higher cumulated P_{micro} in the "High Bloom" trophic regime than in the "Bloom" trophic regime (cumulated "High Bloom" P_{micro} 19 % larger than "Bloom" P_{micro}, Figure 9b), and by a higher cumulated P_{nano} and P_{pico} in the "Bloom" trophic regime compared to the "High Bloom" trophic regime (Figure 9c).

4 Discussion

An analysis of satellite ocean color images revealed the existence in the NWM of two trophic regimes, referred to as "Bloom" and "High Bloom" (Figure 2, [*Mayot et al.*, 2016]). The magnitude of the spring bloom observed in both regimes, when expressed in terms of annual maximum of [Chl-a], is generally larger in the "High Bloom" than in the "Bloom" trophic regime [*Mayot et al.*, 2016]. The "Bloom" trophic regime occurs almost systematically for each of the 16 years considered in the present study, although its spatial extension presents a strong inter-annual variability, whereas the "High Bloom" regime occurs during years with deep convection events. During the DEWEX cruises (2012/13 period), the two trophic regimes were both detected in the NWM, and the spatial extension of the "High Bloom" trophic regime was one of the largest recorded over the 16-year period. The *in situ* data collected during the DEWEX cruises in both trophic regimes confirmed a major difference in the magnitude of the spring [Chl-a] peaks, in the wintertime MLD maximum, and pointed to a difference in the structure of phytoplankton communities in spring (Figure 3). The time-series of HPLC pigment data from the DYFAMED/BOUSSOLE site (Figure 5) displayed similar patterns both in terms of magnitude of the spring [Chl-a] values, in the wintertime MLD and of phytoplankton community structure. A climatological time-series of the two trophic regimes was obtained by merging the DEWEX and DYFAMED/BOUSSOLE data sets (Figure 7). We now use the merged dataset to discuss the role of the phytoplankton community structure in (1) determining the spring production, (2) shaping the seasonal cycle

of primary production, and (3) modulating the inter-annual variability of primary production of the NWM.

The seasonality of the community structure for the two trophic regimes (Figure 7c-d), which is clearly similar during most of the year, begins to diverge in spring, when the [Chl-a] increases over the whole NWM basin. The early stage (i.e. in March) of this spring enhancement of the phytoplankton biomass coincides with an increase in the micro-phytoplankton fraction (Figure 7c-d). The $[\mathrm{Fuco}/(\mathrm{Fuco} + \mathrm{Perid})] \times 100$ pigment ratio (in %) shows that the spring peak of micro-phytoplankton observed in both trophic regimes is mainly composed of diatoms (> 95 % in spring). The occurrence of diatoms during the initial phase of the spring bloom of the NWM has already been reported in the past [*Siokou-Frangou et al.*, 2010; *Estrada and Vaqué*, 2014] and it is generally associated to high values of [Chl-a] [*Marty and Chiavérini*, 2010; *Estrada et al.*, 2014; *Severin et al.*, 2014]. The present results confirm these previous findings, additionally indicating that the "High Bloom" trophic regime shows higher (+ 38 %) spring values of diatoms (58 mg m^{-2}, 96 % of the $[\text{Chl-a}]_{micro}$ = 60 mg m^{-2}) than the "Bloom" trophic regime (36 mg m^{-2}, 90 % of the $[\text{Chl-a}]_{micro}$ = 40 mg m^{-2}). The hypothesis here is that large biomass of diatoms are rather related to the occurrence of the "High Bloom" trophic regime than that of the "Bloom" trophic regime. This hypothesis will be revisited further on.

In a second stage of the spring bloom (i.e. in April), an increase in the nano-phytoplankton fraction is recorded in both trophic regimes, with similar values of biomass for the two trophic regimes (30 mg m^{-2}, Figure 7c-d). The seasonality of nano-phytoplankton is therefore nonspecific to or independent on the trophic regime (i.e. homogenous over the whole NWM area). In view of the sporadic occurrence of the "High Bloom" trophic regime (i.e. occurs during years with deep convection events) this suggests that the presence of nano-phytoplankton in spring could be related to a low inter-annual variability. Independent data from a sediment trap at 500 m in a mooring line deployed at 1000 m and situated in the Gulf of Lion, have indeed confirmed this hypothesis. The coccolith fluxes (originated from coccolithophores species, which belong to nanophytoplankton) at 500 m recorded between 1993 and 2006 by the sediment trap exhibited a stable annual pattern with maximum values during the winter–spring bloom [*Rigual-Hernández et al., 2013*].

Differences in community structure between the two trophic regimes have now been shown to have a role on primary production. Our estimates of the annual primary production for the two trophic regimes are within the range of previous estimations in the NWM area: 180 gC m^{-2} for the "Bloom" trophic regime and 191 gC m^{-2} for the "High Bloom" trophic regime. This 6% difference is within the uncertainty of the light-photosynthesis model [*Morel*, 1991; *Uitz et al.*, 2008], so that the two trophic regimes are assumed to have similar annual primary production rates. This statement does not apply when the primary production is separately analyzed for the three phytoplankton size classes (P_{micro}, P_{nano} and P_{pico}). Present results indicate that the daily primary production in spring due to micro-phytoplankton (P_{micro}) is larger in the "High Bloom" trophic regime (0.8 gC m^{-2}) than in the "Bloom" trophic regime (0.4 gC m^{-2}). Therefore, although the annual primary production appears to be insensitive to the trophic regime, the presence of the "High Bloom" trophic regime was observed to induce a dominance of a micro-phytoplankton production (in particular diatoms) in spring.

The spring bloom represents a critical input of organic matter for the planktonic ecosystem [*Legendre and Le Fèvre*, 1991] and for the sinking of POC to deep waters [*Boyd and Newton*, 1999]. Therefore, an increase in diatom production at this season is certainly critical for the carbon budget of the region, as already shown at a global scale [*Guidi et al.*, 2009, 2015; *Henson et al.*, 2012] and in the NWM [*Rigual-Hernández et al.*, 2013; *Ramondenc et al.*, 2016].

The amount of organic carbon annually produced for the "Bloom" and "High Bloom" trophic regimes has been calculated by multiplying their climatological annual rates of primary production (180 gC m^{-2} for the "Bloom" trophic regime, and 191 gC m^{-2} for the "High Bloom" trophic regime) by the surface area they cover. On average, the annual stock of organic carbon produced in the NWM is 18.9 TgC ± 9 TgC (dashed line Figure 10a). Values about 50 % above this average are however observed in 1998/99, 2004/05, 2005/06, 2009/10 and 2012/13 (on average, 29.5 TgC ± 5 TgC), when the spatial extent of the "High Bloom" regime was maximal. During the same years, the surface area of the blooming region (i.e. the area covered by both trophic regimes, Figure 2) is also larger than that of the 16-year average (+ 155 %). Moreover, the mean value of the amount of organic carbon produced in spring by the micro-phytoplankton (between March and May, Figure 10c) is enhanced during these highly productive years (4.4 TgC ± 0.8 TgC, compared to the mean value of 2.7 TgC ± 1.4 TgC, + 63 %).

Given these results, it can be expected that the proportion of micro-phytoplankton (mainly diatoms) in the spring phytoplankton community and, consequently, the amount of POC exported at depth in spring in the NWM, should increase when conditions inducing the "High Bloom" regime appear. As the "High Bloom" regime is associated with particularly cold and windy winters and very deep winter mixed layers [*Mayot et al.*, 2016; *Mayot et al.,* submitted] (Figure 7e-f and 10b), a direct relationship could exist between the winter hydrodynamic-atmospheric conditions of the NWM and the enhanced spring diatom production, which is generally correlated with the POC exported at depth [*Guidi et al.*, 2009, 2015; *Henson et al.*, 2012]. The presence of diatoms during the spring bloom in the NWM has already been observed to increase during years characterized by particularly cold winters [*Rigual-Hernández et al.*, 2013; *Organelli et al.*, 2013]. The general hypothesis implies that, during extremely cold winters, the mixed layer is deeper (MLD reaches the bottom, [*Houpert et al.*, 2016]), which induces an increase in the nutrient availability in the surface layer, thereby favoring the growth of diatoms in the springtime. As the stoichiometric ratio between silicates and nitrates can be positively affected by strong winter mixing (more silicate than nitrate, [*Severin et al.*, 2014]), cold and windy winters could be characterized by an increase in the silicate availability in the surface layer, which, in turn, could also support the development of a diatom bloom in spring. The occurrence of the "High Bloom" trophic regime, which is associated with deep winter mixed layers and high biomass of diatoms in spring, could be used as a proxy to identify a shift in the phytoplankton community structure in spring.

As a consequence, an increased frequency of warm and dry conditions in the NWM region, as currently predicted by coupled ocean-ecosystem models [*IPCC, 2014; Mariotti et al., 2015*], may lead to a reduction in deep winter mixed layers [*Adloff et al., 2015*]. However, these results from model projections appear strongly modulated by the Atlantic forcing at the boundary conditions (the warming and the saltening applied to the Atlantic water in the general circulation models), and less by the choice of the socio-economic scenario [*Adloff et*

al., 2015]. Considering only the scenario A2 [*IPCC, 2014*], several model-based studies, which used different ocean climate models (i.e. [*Somot et al., 2006; Adloff et al., 2015*]), tended to report a decrease of the deep convection activity in the Gulf of Lion related to an increase of the vertical stratification. In addition, results from annual simulations of a 3D coupled physical-biogeochemical model performed under future climate conditions suggested a potential biomass increase of smaller plankton size classes (bacteria, pico-phytoplankton and nano-zooplankton) [*Herrmann et al., 2014*]. In turn, a potential diminution of the wintertime and springtime organic carbon exported to the deep ocean can be expected.

During winter deep convection, as in the NWM, part of the organic carbon exported to the deep prevails in a dissolved form (DOC, [*Hansell et al.*, 2009; *Carlson et al.*, 2010; *Santinelli et al.*, 2010]) and was estimated to be up to 88 % in the NWM [*Ramondenc et al.*, 2016]. Therefore a lower occurrence of intense deep convection events could induce a reduction of the biological carbon pump *via* the diminution of the POC and DOC exported to depth. However, a causal relationship between biological production and organic carbon flux to deep waters is still a subject of debate (e.g. [*Passow and Carlson*, 2012]). Another way to sequester carbon involving DOC is the microbial carbon pump, which corresponds to the production, mainly by microbial organisms, of long-lived DOC (recalcitrant DOC with a life time longer than 100 years) [*Jiao et al.*, 2010; *Legendre et al.*, 2015]. However, climate-driven changes in the oceanic environment could enhance or reduce the production of long-lived recalcitrant DOC [*Legendre et al.*, 2015]. Therefore, an estimation of the overall potential effects of climate changes on both the biological and the microbial carbon pumps, and finally on the carbon sequestered, require more investigations and extensive modeling studies.

5 Conclusion

The phytoplankton community structure has been analyzed in the NWM using phytoplankton pigment data. Moreover, a spatial division of the NWM into trophic regimes (ecological units), based on satellite-derived [Chl-a], has been applied to give a meaningful context to this analysis. Two main trophic regimes can be detected in the NWM: the “Bloom” and the “High Bloom” trophic regimes. The *in situ* data of phytoplankton pigments demonstrated temporal and magnitude differences between the spring blooms of these two trophic regimes. In addition, the enhanced spring bloom of the “High Bloom” trophic regime is related to an increase in the diatom biomass maximum in spring. On the contrary, the spring biomass maximum of nano-phytoplankton remains similar between the two trophic regimes, and always occurs after the diatom spring peak. This suggests that the increase in the phytoplankton biomass maximum during spring could be related to a larger diatom contribution.

The primary production associated with the two trophic regimes has been quantified with a phytoplankton-class-specific light-photosynthesis model. The maximum rate of daily primary production occurs in spring. It is higher in the “High Bloom” trophic regime than in the “Bloom” trophic regime (+ 0.5 gC m^{-2}, + 45 %). The values of annual primary production associated with the two trophic regimes are however undistinguishable (only a difference of 11 gC m^{-2} or 6 % difference). The daily primary production in spring associated with diatoms is enhanced in the “High Bloom” trophic regime (+ 0.4 gC m^{-2}, + 100 %). This could have an impact on the flux of POC exported to the deep.

The "High Bloom" trophic regime in the NWM is associated to an increase in the stock of organic material produced throughout the whole NWM sub-basin (+ 10.6 TgC, + 56 %), and to an increase of the primary production by micro-phytoplankton (+ 1.7 TgC, + 63 %). This trophic regime is associated to years of intense deep convection generated by colder-than-average winters, suggesting that an increase of warm and dry conditions in the NWM, as predicted by climate change scenarios, could affect the amount of organic carbon exported to depth in spring.

Acknowledgements

This work is a contribution to the MerMEX project (Marine Ecosystem Response in the Mediterranean Experiment, WP1) of the MISTRALS international program (Mediterranean Integrated Studies at Regional and Local Scales). This work was supported by the remOcean project (remotely sensed biogeochemical cycles in the Ocean), funded by the European Research Council (GA 246777), by the French "Equipement d'avenir" NAOS project (Novel Argo Ocean observing System, ANR J11R107-F), and by the region *Provence Alpes Côte d'Azur*. The GlobColour data set used is available on the ACRI-ST website (http://hermes.acri.fr/index.php?class=archive). We thank the members of the SAPIGH platform (Analytical Service dedicated to High quality measurements of phytoplankton Pigments) from the *Laboratoire d'Océanographie de Villefranche* for the HPLC analysis. The authors acknowledge the NASA Ocean Biology Processing Group for the access to SeaWiFS (Sea-Viewing Wide Field-of-View Sensor) and MODIS (Moderate Resolution Imaging Spectroradiometer) data (http://oceancolor.gsfc.nasa.gov). Finally, we are grateful to two anonymous reviewers for their valuable comments and suggestions.

References

Antoine, D., A. Morel, and J. M. André (1995), Algal pigment distribution and primary production in the eastern Mediterranean as derived from coastal zone color scanner observations, *J. Geophys. Res. Ocean.*, *100*(C8), 16193–16209.

Antoine, D. et al. (2006), BOUSSOLE : A Joint CNRS-INSU, ESA, CNES, and NASA Ocean Color Calibration and Validation Activity, *NASA Tech. Memo.*, *2006–21414*, 59.

Antoine, D., F. d'Ortenzio, S. B. Hooker, G. Bécu, B. Gentili, D. Tailliez, and A. J. Scott (2008), Assessment of uncertainty in the ocean reflectance determined by three satellite ocean color sensors (MERIS, SeaWiFS and MODIS-A) at an offshore site in the Mediterranean Sea (BOUSSOLE project), *J. Geophys. Res. Ocean.*, *113*(C7).

Arin, L., J. Guillén, M. Segura-Noguera, and M. Estrada (2013), Open sea hydrographic forcing of nutrient and phytoplankton dynamics in a Mediterranean coastal ecosystem, *Estuar. Coast. Shelf Sci.*, *133*, 116–128, doi:10.1016/j.ecss.2013.08.018.

Auger, P. A., C. Ulses, C. Estournel, L. Stemmann, S. Somot, and F. Diaz (2014), Interannual control of plankton communities by deep winter mixing and prey/predator interactions in the NW Mediterranean: Results from a 30-year 3D modeling study, *Prog. Oceanogr.*, *124*, 12–27.

Barnard, A. H., and T. O. Mitchell (2013), Biogeochemical monitoring of the oceans using autonomous profiling floats, *Ocean News Technol*, *19*(2), 16–17.

Bosc, E., A. Bricaud, and D. Antoine (2004), Seasonal and interannual variability in algal biomass and primary production in the Mediterranean Sea, as derived from 4 years of

SeaWiFS observations, *Global Biogeochem. Cycles*, *18*(1), GB1005, doi:10.1029/2003GB002034.

Bouman, H., T. Platt, and S. Sathyendranath (2005), Dependence of light-saturated photosynthesis on temperature and community structure, *Deep Sea Res. Part I*.

Boyd, P. W., and P. P. Newton (1999), Does planktonic community structure determine downward particulate organic carbon flux in different oceanic provinces?, *Deep Sea Res. Part I Oceanogr. Res. Pap.*, *46*(1), 63–91, doi:10.1016/S0967-0637(98)00066-1.

Brewin, R. J. W., S. J. Lavender, and N. J. Hardman-Mountford (2010), Mapping size-specific phytoplankton primary production on a global scale, *J. Maps*, *6*(1), 448–462, doi:10.4113/jom.2010.1122.

Carlson, C. A., N. B. Nelson, D. A. Siegel, W. M. Smethie, S. Khatiwala, M. M. Meyers, and E. Halewood (2010), Dissolved organic carbon export and subsequent remineralization in the mesopelagic and bathypelagic realms of the North Atlantic basin, *Deep Sea Res. Part II Top. Stud. Oceanogr.*, *57*(16), 1433–1445, doi:10.1016/j.dsr2.2010.02.013.

Claustre, H. (1994), The trophic status of various oceanic provinces as revealed by phytoplankton pigment signatures, *Limnol. Oceanogr.*, *39*(5), 1206–1210, doi:10.4319/lo.1994.39.5.1206.

Coppola, L., E. Diamond Riquier, and T. Carval (2016), Dyfamed observatory data, , doi:10.17882/43749.

D'Ortenzio, F., S. Le Reste, H. Lavigne, F. Besson, H. Claustre, L. Coppola, A. Dufour, V. Dutreuil, A. Laes, and E. Leymarie (2012), Autonomously profiling the nitrate concentrations in the ocean: The Pronuts project, *Mercat. Ocean. Q. Newsl.*, (45), 8–11.

Edwards, K. F., M. K. Thomas, C. A. Klausmeier, and E. Litchman (2015), Light and growth in marine phytoplankton: allometric, taxonomic, and environmental variation, *Limnol. Oceanogr.*, *60*(2), 540–552.

Estrada, M. (1996), Primary production in the northwestern Mediterranean, *Sci. Mar.*, *60*(S2), 55–64.

Estrada, M., and D. Vaqué (2014), Microbial components, in *The Mediterranean Sea*, pp. 87–111, Springer.

Estrada, M., M. Latasa, M. Emelianov, A. Gutiérrez-Rodríguez, B. Fernández-Castro, J. Isern-Fontanet, B. Mouriño-Carballido, J. Salat, and M. Vidal (2014), Seasonal and mesoscale variability of primary production in the deep winter-mixing region of the NW Mediterranean, *Deep Sea Res. Part I Oceanogr. Res. Pap.*, *94*, 45–61.

Guidi, L., L. Stemmann, and G. Jackson (2009), Effects of phytoplankton community on production, size, and export of large aggregates: A world-ocean analysis, *Limnol.*

Guidi, L., L. Legendre, G. Reygondeau, J. Uitz, L. Stemmann, and S. A. Henson (2015), A new look at ocean carbon remineralization for estimating deepwater sequestration, *Global Biogeochem. Cycles*, *29*(7), 1044–1059, doi:10.1002/2014GB005063.

Hansell, D., C. Carlson, D. Repeta, and R. Schlitzer (2009), Dissolved Organic Matter in the Ocean: A Controversy Stimulates New Insights, *Oceanography*, *22*(4), 202–211, doi:10.5670/oceanog.2009.109.

Henson, S. A., R. Sanders, and E. Madsen (2012), Global patterns in efficiency of particulate

organic carbon export and transfer to the deep ocean, *Global Biogeochem. Cycles*, *26*(1), n/a-n/a, doi:10.1029/2011GB004099.

Herrmann, M., F. Diaz, C. Estournel, P. Marsaleix, and C. Ulses (2013), Impact of atmospheric and oceanic interannual variability on the Northwestern Mediterranean Sea pelagic planktonic ecosystem and associated carbon cycle, *J. Geophys. Res. Ocean.*, *118*(10), 5792–5813, doi:10.1002/jgrc.20405.

Heussner, S., X. Durrieu de Madron, A. Calafat, M. Canals, J. Carbonne, N. Delsaut, and G. Saragoni (2006), Spatial and temporal variability of downward particle fluxes on a continental slope: Lessons from an 8-yr experiment in the Gulf of Lions (NW Mediterranean), *Mar. Geol.*, *234*(1), 63–92, doi:10.1016/j.margeo.2006.09.003.

Hood, R. R. et al. (2006), Pelagic functional group modeling: Progress, challenges and prospects, *Deep Sea Res. Part II Top. Stud. Oceanogr.*, *53*(5), 459–512, doi:10.1016/j.dsr2.2006.01.025.

Houpert, L. et al. (2016), Observations of open-ocean deep convection in the northwestern Mediterranean Sea : Seasonal and interannual variability of mixing and deep water masses for the 2007-2013 period, *J. Geophys. Res. Ocean.*, doi:10.1002/2016JC011857.

Ipcc (2013), Working Group I Contribution to the IPCC Fifth Assessment Report, Climate Change 2013: The Physical Science Basis, *Ipcc*, *AR5*(March 2013), 2014, doi:10.1017/CBO9781107415324.Summary.

Jiao, N. et al. (2010), Microbial production of recalcitrant dissolved organic matter: long-term carbon storage in the global ocean, *Nat. Rev. Microbiol.*, *8*(8), 593–599, doi:10.1038/nrmicro2386.

Lavigne, H., F. D'Ortenzio, C. Migon, H. Claustre, P. Testor, M. R. d'Alcala, R. Lavezza, L. Houpert, and L. Prieur (2013), Enhancing the comprehension of mixed layer depth control on the Mediterranean phytoplankton phenology, *J. Geophys. Res. Ocean.*, *118*, 3416–3430, doi:10.1002/jgrc.20251.

Legendre, L., and J. Le Fèvre (1991), From Individual Plankton Cells To Pelagic Marine Ecosystems And To Global Biogeochemical Cycles, in *Particle Analysis in Oceanography*, pp. 261–300, Springer Berlin Heidelberg, Berlin, Heidelberg.

Legendre, L., R. B. Rivkin, M. G. Weinbauer, L. Guidi, and J. Uitz (2015), The microbial carbon pump concept: Potential biogeochemical significance in the globally changing ocean, *Prog. Oceanogr.*, *134*, 432–450, doi:10.1016/j.pocean.2015.01.008.

Lewis, M. R., R. E. Warnock, B. Irwin, and T. Platt (1985), Measuring photosynthetic action spectra of natural phytoplankton population, *J. Phycol.*, *21*(2), 310–315, doi:10.1111/j.0022-3646.1985.00310.x.

Mariotti, A., Y. Pan, N. Zeng, and A. Alessandri (2015), Long-term climate change in the Mediterranean region in the midst of decadal variability, *Clim. Dyn.*, *44*(5–6), 1437–1456, doi:10.1007/s00382-015-2487-3.

Marty, J., and J. Chiavérini (2002), Seasonal and interannual variations in phytoplankton production at DYFAMED time-series station, northwestern Mediterranean Sea, *Deep Sea Res. Part II Top. Stud.*

Marty, J.-C., J. Chiavérini, M.-D. Pizay, and B. Avril (2002), Seasonal and interannual dynamics of nutrients and phytoplankton pigments in the western Mediterranean Sea at

the DYFAMED time-series station (1991–1999), *Deep Sea Res. Part II Top. Stud. Oceanogr.*, *49*(11), 1965–1985, doi:10.1016/S0967-0645(02)00022-X.

Marty, J. C., and J. Chiavérini (2010), Hydrological changes in the Ligurian Sea (NW Mediterranean, DYFAMED site) during 1995–2007 and biogeochemical consequences, *Biogeosciences*, *7*(7), 2117–2128.

Mayot, N., F. D'Ortenzio, M. Ribera d'Alcalà, H. Lavigne, and H. Claustre (2016), Interannual variability of the Mediterranean trophic regimes from ocean color satellites, *Biogeosciences*, *13*, 1901–1917.

MEDOC Group (1970), Observation of Formation of Deep Water in the Mediterranean Sea, 1969, *Nature*, *227*(5262), 1037–1040, doi:10.1038/2271037a0.

Michaels, A. F., A. H. Knap, R. L. Dow, K. Gundersen, R. J. Johnson, J. Sorensen, A. Close, G. A. Knauer, S. E. Lohrenz, and V. A. Asper (1994), Seasonal patterns of ocean biogeochemistry at the US JGOFS Bermuda Atlantic Time-series Study site, *Deep Sea Res. Part I Oceanogr. Res. Pap.*, *41*(7), 1013–1038.

Millot, C. (1999), Circulation in the Western Mediterranean Sea, *J. Mar. Syst.*, *20*(1), 423–442, doi:10.1016/S0924-7963(98)00078-5.

Miquel, J.-C., J. Martín, B. Gasser, A. Rodriguez-y-Baena, T. Toubal, and S. W. Fowler (2011), Dynamics of particle flux and carbon export in the northwestern Mediterranean Sea: A two decade time-series study at the DYFAMED site, *Prog. Oceanogr.*, *91*(4), 461–481, doi:10.1016/j.pocean.2011.07.018.

Morel, A. (1988), Optical modeling of the upper ocean in relation to its biogenous matter content (case I waters), *J. Geophys. Res.*, *93*(C9), 10749, doi:10.1029/JC093iC09p10749.

Morel, A. (1991), Light and marine photosynthesis: a spectral model with geochemical and climatological implications, *Prog. Oceanogr.*, *26*(3), 263–306, doi:10.1016/0079-6611(91)90004-6.

Morel, A., and J. M. André (1991), Pigment distribution and primary production in the western Mediterranean as derived and modeled from Coastal Zone Color Scanner observations, *J. Geophys. Res. Ocean.*, *96*(C7), 12685–12698, doi:10.1029/91JC00788.

Morel, A., and J. F. Berthon (1989), Surface pigments, algal biomass profiles, and potential production of the euphotic layer: Relationships reinvestigated in view of remote-sensing applications, *Limnol. Oceanogr.*, *34*(8), 1545–1562.

Morel, A., and S. Maritorena (2001), Bio-optical properties of oceanic waters: A reappraisal, *J. Geophys. Res. Ocean.*, *106*(C4), 7163–7180, doi:10.1029/2000JC000319.

Morel, A., Y. Huot, B. Gentili, P. J. Werdell, S. B. Hooker, and B. A. Franz (2007), Examining the consistency of products derived from various ocean color sensors in open ocean (Case 1) waters in the perspective of a multi-sensor approach, *Remote Sens. Environ.*, *111*(1), 69–88.

Niewiadomska, K., H. Claustre, L. Prieur, and F. d'Ortenzio (2008), Submesoscale physical-biogeochemical coupling across the Ligurian current (northwestern Mediterranean) using a bio-optical glider, *Limnol. Oceanogr.*, *53*(5), 2210.

Olita, A., R. Sorgente, A. Ribotti, L. Fazioli, and A. Perilli (2011a), Pelagic primary

production in the Algero-Provençal Basin by means of multisensor satellite data: focus on interannual variability and its drivers, *Ocean Dyn.*, *61*(7), 1005–1016, doi:10.1007/s10236-011-0405-8.

Olita, A., A. Ribotti, R. Sorgente, L. Fazioli, and A. Perilli (2011b), SLA–chlorophyll-a variability and covariability in the Algero-Provençal Basin (1997–2007) through combined use of EOF and wavelet analysis of satellite data, *Ocean Dyn.*, *61*(1), 89–102.

Omand, M. M., E. A. D'Asaro, C. M. Lee, M. J. Perry, N. Briggs, I. Cetini , and A. Mahadevan (2015), Eddy-driven subduction exports particulate organic carbon from the spring bloom, *Science (80-.).*, *348*(6231), 222–225, doi:10.1126/science.1260062.

Passow, U., and C. Carlson (2012), The biological pump in a high CO2 world, *Mar. Ecol. Prog. Ser.*, *470*, 249–271, doi:10.3354/meps09985.

Platt, T., C. L. Gallegos, and W. G. Harrison (1980), Photoinibition of photosynthesis in natural assemblages of marine phytoplankton, *J. Mar. Res.*, *38*, 687–701.

Poulain, P.-M., R. Barbanti, J. Font, A. Cruzado, C. Millot, I. Gertman, A. Griffa, A. Molcard, V. Rupolo, and S. Le Bras (2007), MedArgo: a drifting profiler program in the Mediterranean Sea, *Ocean Sci.*, *3*(3), 379–395.

Quere, C. Le et al. (2005), Ecosystem dynamics based on plankton functional types for global ocean biogeochemistry models, *Glob. Chang. Biol.*, *0*(0), 051013014052005–???, doi:10.1111/j.1365-2486.2005.1004.x.

Ramondenc, S., G. Madeleine, F. Lombard, C. Santinelli, L. Stemmann, G. Gorsky, and L. Guidi (2016), An initial carbon export assessment in the Mediterranean Sea based on drifting sediment traps and the Underwater Vision Profiler data sets, *Deep Sea Res. Part I Oceanogr. Res. Pap.*, doi:10.1016/j.dsr.2016.08.015.

Ras, J., H. Claustre, and J. Uitz (2008), Spatial variability of phytoplankton pigment distributions in the Subtropical South Pacific Ocean: comparison between in situ and predicted data, *Biogeosciences*, *5*(2), 353–369.

Richardson, T. L., and G. A. Jackson (2007), Small Phytoplankton and Carbon Export from the Surface Ocean, *Science (80-.).*, *315*(5813).

Rigual-Hernández, A. S., M. A. Bárcena, R. W. Jordan, F. J. Sierro, J. A. Flores, K. J. S. Meier, L. Beaufort, and S. Heussner (2013), Diatom fluxes in the NW Mediterranean: evidence from a 12-year sediment trap record and surficial sediments, *J. Plankton Res.*, *35*(5), 1109–1125.

San Feliu, J. M., and F. Muñoz (1971), Fluctuations d'une année à l'autre dans l'intensité de l'affleurement dans la Méditerranée occidentale, *Invest. pesq.*, *35*(1), 155–159.

Santinelli, C., L. Nannicini, and A. Seritti (2010), DOC dynamics in the meso and bathypelagic layers of the Mediterranean Sea, *Deep Sea Res. Part II Top. Stud. Oceanogr.*, *57*(16), 1446–1459, doi:10.1016/j.dsr2.2010.02.014.

Severin, T., P. Conan, X. Durrieu de Madron, L. Houpert, M. J. Oliver, L. Oriol, J. Caparros, J. F. Ghiglione, and M. Pujo-Pay (2014), Impact of open-ocean convection on nutrients, phytoplankton biomass and activity, *Deep Sea Res. Part I Oceanogr. Res. Pap.*, *94*, 62–71, doi:10.1016/j.dsr.2014.07.015.

Siokou-Frangou, I., U. Christaki, M. G. Mazzocchi, M. Montresor, M. Ribera d'Alcalá, D.

Vaqué, and A. Zingone (2010), Plankton in the open Mediterranean Sea: a review, *Biogeosciences*, *7*(5), 1543–1586, doi:10.5194/bg-7-1543-2010.

Stabholz, M. et al. (2013), Impact of open-ocean convection on particle fluxes and sediment dynamics in the deep margin of the Gulf of Lions, *Biogeosciences*, *10*(2), 1097–1116, doi:10.5194/BG-10-1097-2013.

Testor, P. et al. (2010), Gliders as a Component of Future Observing Systems, in *Proceedings of OceanObs'09: Sustained Ocean Observations and Information for Society*, pp. 961–978, European Space Agency.

The Mermex Group (2011), Marine ecosystems' responses to climatic and anthropogenic forcings in the Mediterranean, *Prog. Oceanogr.*, *91*(2), 97–166, doi:10.1016/j.pocean.2011.02.003.

Le Traon, P.-Y., F. D'Ortenzio, M. Babin, H. Claustre, S. Pouliquen, S. Le Reste, V. Thierry, P. Brault, M. Guigue, and M. Le Menn (2012), NAOS: preparing the new decade for Argo, *Mercat. Ocean. Q. Newsl.*, (45), 3–4.

Uitz, J., H. Claustre, A. Morel, and S. B. Hooker (2006), Vertical distribution of phytoplankton communities in open ocean: An assessment based on surface chlorophyll, *J. Geophys. Res.*, *111*(C8), C08005, doi:10.1029/2005JC003207.

Uitz, J., Y. Huot, F. Bruyant, M. Babin, and H. Claustre (2008), Relating phytoplankton photophysiological properties to community structure on large scales, *Limnol. Oceanogr.*, *53*(2), 614–630, doi:10.4319/lo.2008.53.2.0614.

Uitz, J., D. Stramski, B. Gentili, F. D'Ortenzio, and H. Claustre (2012), Estimates of phytoplankton class specific and total primary production in the Mediterranean Sea from satellite ocean color observations, *Global Biogeochem. Cycles*, *26*(2), GB2024, doi:10.1029/2011GB004055.

Ulses, C., P.-A. Auger, K. Soetaert, P. Marsaleix, F. Diaz, L. Coppola, M. J. Herrmann, F. Kessouri, and C. Estournel (2016), Budget of organic carbon in the North-Western Mediterranean Open Sea over the period 2004-2008 using 3-D coupled physical-biogeochemical modeling, *J. Geophys. Res. Ocean.*, doi:10.1002/2016JC011818.

Vidussi, F., H. Claustre, and B. Manca (2001), Phytoplankton pigment distribution in relation to upper thermocline circulation in the eastern Mediterranean Sea during winter, *J.*

Volpe, G., B. B. Nardelli, P. Cipollini, R. Santoleri, and I. S. Robinson (2012), Seasonal to interannual phytoplankton response to physical processes in the Mediterranean Sea from satellite observations, *Remote Sens. Environ.*, *117*, 223–235.

Table 1: Summary of the number of stations used for this study. Only offshore stations (bathymetry > 1000 m) performed in the two studied trophic regimes are considered. For the BGC-Argo floats and the Bio-optical gliders, the number in parentheses corresponds to the number of chlorophyll-*a* fluorescence profiles available.

	Number of stations	Number of HPLC stations	Sampling period	Reference/DOI
DEWEX Cruises				
MOOSE-GE - 2012	63		Jul. to Aug. 2012	doi: 10.17600/12020030
DOWEX - 2012	36	13	Sep. 2012	doi: 10.17600/13450150
DEWEX - Leg 1	54	15	Feb. 2013	doi: 10.17600/13020010
DEWEX - Leg 2	67	17	Apr. 2013	doi: 10.17600/13020030
MOOSE-GE - 2013	40	10	Jun. to Jul. 2013	doi: 10.17600/13450110
Total	**260**	**55**		
Argo floats	789		Jul. to Jul. 2013	[*Poulain et al.*, 2007]
BGC-Argo floats	305 (240)		Jul. to Jul. 2013	[*D'Ortenzio et al.*, 2012; *Le Traon et al.*, 2012; *Barnard and Mitchell*, 2013]
Bio-optical gliders	2338 (254)		Sep. to Jul. 2013	[*Niewiadomska et al.*, 2008; *Testor et al.*, 2010]
Total	**3432**			
DYFAMED/BOUSSOLE site				
DYFAMED project	57	57	1998 to 2007	doi: 10.17882/43749 [*Coppola et al.*, 2016]
BOUSSOLE project	174	174	2001 to 2014	[*Antoine et al.*, 2006, 2008]
Total	**231**	**231**		

Table 2: Diagnostic pigments used with their taxonomic correspondence, from [*Vidussi et al.*, 2001]

Pigments	Abbreviations	Taxonomic Significance	Phytoplankton size class
Fucoxanthin	Fuco	diatoms	micro- (> 20 µm)
Peridinin	Perid	dinoflagellates	
Alloxanthin	Allo	cryptophytes	nano- (2-20 µm)
19'-butanoyloxyfucoxanthin	ButFuco	chromophytes and nanoflagellates	
19'-hexanoyloxyfucoxanthin	HexFuco	chromophytes and nanoflagellates	
Zeaxanthin	Zea	cyanobacteria and prochlorophytes	pico- (< 2 µm)
Total Chlorophyll-b	TChlb	green flagellates and prochlorophytes	

Figure 1. Map of the NWM showing the location of cruise stations and of the DYFAMED/BOUSSOLE site. Colored areas indicate the spatial location of the two studied trophic regimes in 2012/13 (the "Bloom" and "High Bloom" trophic regimes, from [Mayot et al., 2016]). The mean currents are represented by arrows with continuous lines (WCC: Western Corsican Current, NC: Northern Current) and the North Balearic Front (NBF) by an arrow with a dashed line.

Figure 2. Spatial extent of the "Bloom" (blue) and "High Bloom" (orange) trophic regimes in the NWM and for the years indicated (from [*Mayot et al.*, 2016]). The year is here defined between July to July (e.g. for 1998/99: July 1998 to July 1999). The star in the Ligurian Sea indicates the location of the DYFAMED/BOUSSOLE site.

Figure 3. Annual cycle of total and class-specific $[Chl\text{-}a]_{1.5*Zeu}$, and of the MLD, for the two studied trophic regimes: "Bloom" (a, c and e) and "High Bloom" (b, d and f) between July 2012 and July 2013 (DEWEX cruises). The total $[Chl\text{-}a]_{1.5*Zeu}$ is the sum of each (c-d) class-specific $[Chl\text{-}a]_{1.5*Zeu}$: $[Chl\text{-}a]_{micro}$, $[Chl\text{-}a]_{nano}$ and $[Chl\text{-}a]_{pico}$ (for the micro-, nano- and pico-phytoplankton respectively). The total $[Chl\text{-}a]_{1.5*Zeu}$ was also obtained from fluorometers measurements (black lines). (c-d) The mean class-specific $[Chl\text{-}a]_{1.5*Zeu}$ (with the standard deviation) is calculated for each DEWEX cruises (Table 1). (e-f) The MLD estimations higher or equal to 2000 m are indicated by black dots.

Figure 4. Ternary plots of the seasonal variations between 0 m and $1.5 \times Z_{eu}$ of the fraction of [Chl-a] associated with the three phytoplankton size classes: micro- (f_{micro}), nano- (f_{nano}) and pico-phytoplankton (f_{pico}), for the two studied trophic regimes: "Bloom" (a) and "High Bloom" (b), between July 2012 and July 2013 (DEWEX cruises). Each color represents a season.

Figure 5. Climatological annual cycle of total and class-specific $[Chl\text{-}a]_{1.5*Zeu}$, and of the MLD, for the two studied trophic regimes: "Bloom" (a, c and e) and "High Bloom" (b, d and f) at the DYFAMED/BOUSSOLE site. The total $[Chl\text{-}a]_{1.5*Zeu}$ is the sum of each (c-d) class-specific $[Chl\text{-}a]_{1.5*Zeu}$: $[Chl\text{-}a]_{micro}$, $[Chl\text{-}a]_{nano}$ and $[Chl\text{-}a]_{pico}$ (for the micro-, nano- and pico-phytoplankton respectively). (e-f) For the BOUSSOLE project (black points), the maximum possible MLD value is 400 m (the greatest depth of the CTD cast).

Figure 6. Ternary plots of the climatological seasonal variations between 0 m and $1.5 \times Z_{eu}$ of the fraction of the [Chl-a] associated with the three phytoplankton size classes: micro- (f_{micro}), nano- (f_{nano}) and pico-phytoplankton (f_{pico}), for the two studied trophic regimes: "Bloom" (a) and "High Bloom" (b), at the DYFAMED/BOUSSOLE site. Each color represents a season.

Figure 7. Climatological annual cycle of total and class-specific $[Chl\text{-}a]_{1.5*Zeu}$, and of the MLD, for the two studied trophic regimes: "Bloom" (a, c and e) and "High Bloom" (b, d and f). The total $[Chl\text{-}a]_{1.5*Zeu}$ is the sum of each (c-d) class-specific $[Chl\text{-}a]_{1.5*Zeu}$: $[Chl\text{-}a]_{micro}$, $[Chl\text{-}a]_{nano}$ and $[Chl\text{-}a]_{pico}$ (for the micro-, nano- and pico-phytoplankton respectively). (e-f) For the BOUSSOLE project (black points), the maximum possible MLD value is 400 m (the greatest depth of the CTD cast).

Figure 8. Climatological annual cycle of total and class-specific daily primary production for the two studied trophic regimes, obtained from the light-photosynthesis model. (a-b) The total primary production is the sum of (c-d) each class-specific primary production: P_{micro}, P_{nano} and P_{pico} (for the micro-, nano- and pico-phytoplankton respectively). These results are displayed separately for the "Bloom" (a and c) and "High Bloom" (b and d) trophic regimes.

Figure 9. Climatological annual cycle of cumulative total and class-specific primary production for the two studied trophic regimes obtained from the light-photosynthesis model. Each class-specific primary production: (b) P_{micro}, (c) P_{nano} and (d) P_{pico} (for the micro-, nano- and pico-phytoplankton respectively), is expressed in percentage of (a) the total primary production (P_{tot}).

Figure 10. Estimation of (a) annual and (c) spring primary production at basin-scale for the NWM, and of the winter MLD (b). (a) The basin scale estimate of annual primary production (P_{NWM}) is the

sum of both P_{Bloom} and $P_{High\ Bloom}$ (i.e. the annual primary production associated with the two trophic regimes). The average value of P_{NWM} is 18.9 TgC (black dashed line). (b) Inter-annual boxplot of the winter MLD with all estimations available (in grey) in the two trophic regimes. (c) The spring primary production (between March and May) for micro- (P_{micro}), nano- (P_{nano}) and pico-phytoplankton (P_{pico}).

Figure 1.

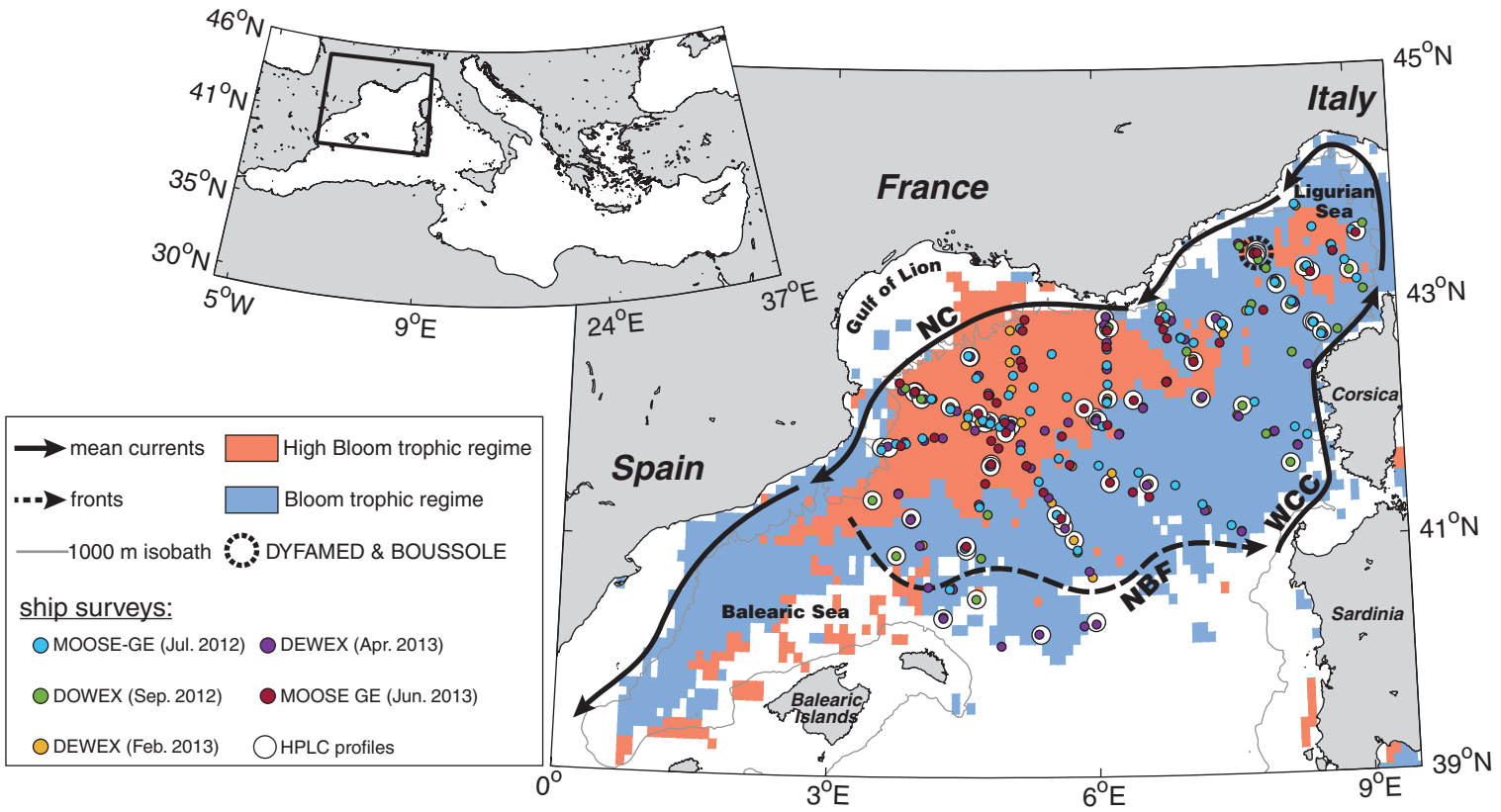

Figure 2.

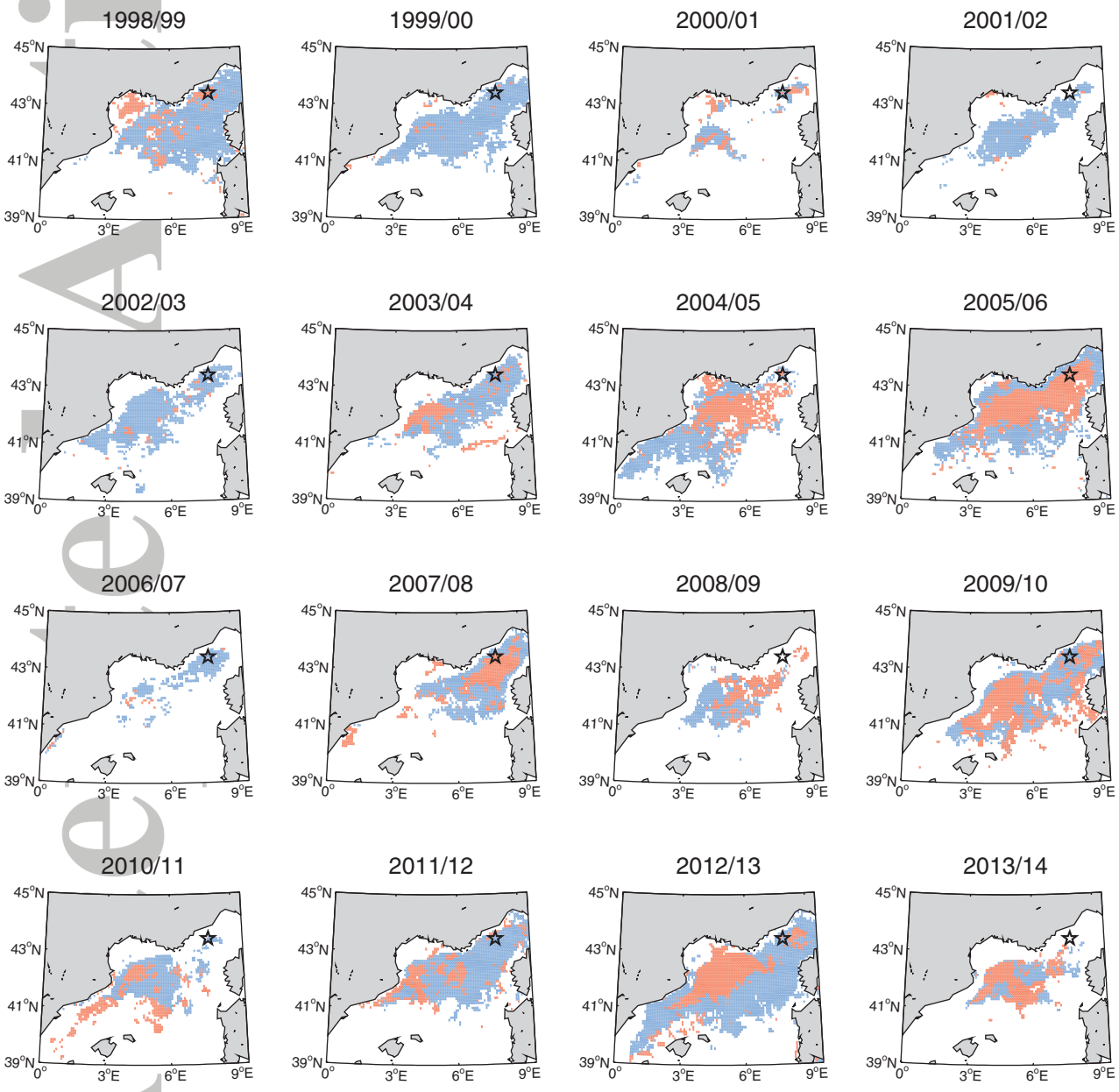

Figure 3.

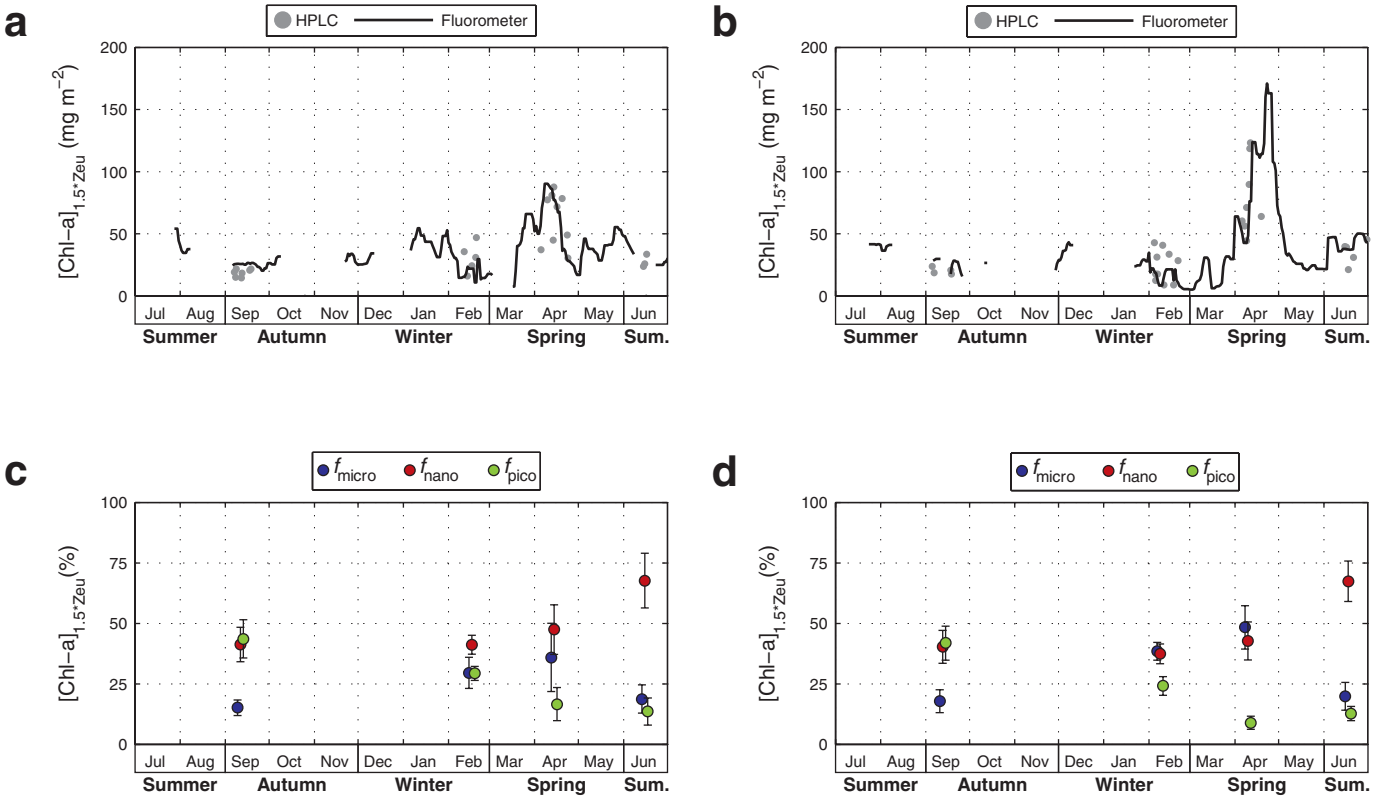

Figure 4.

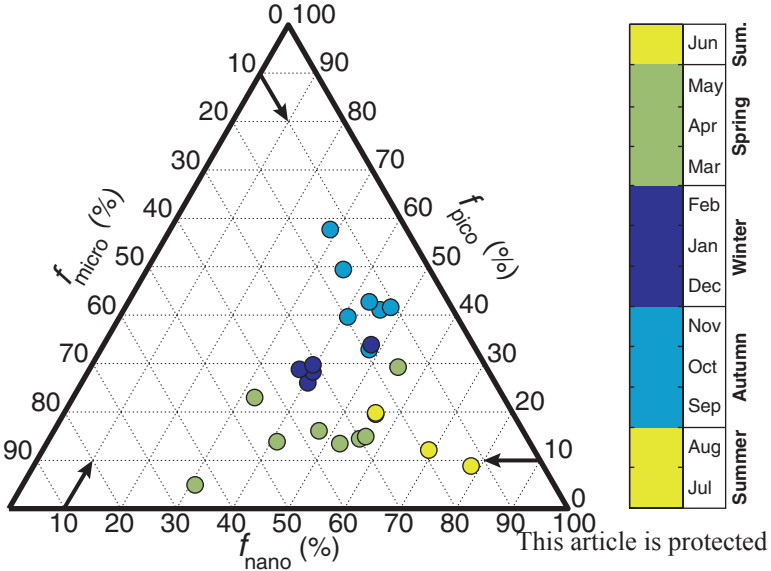

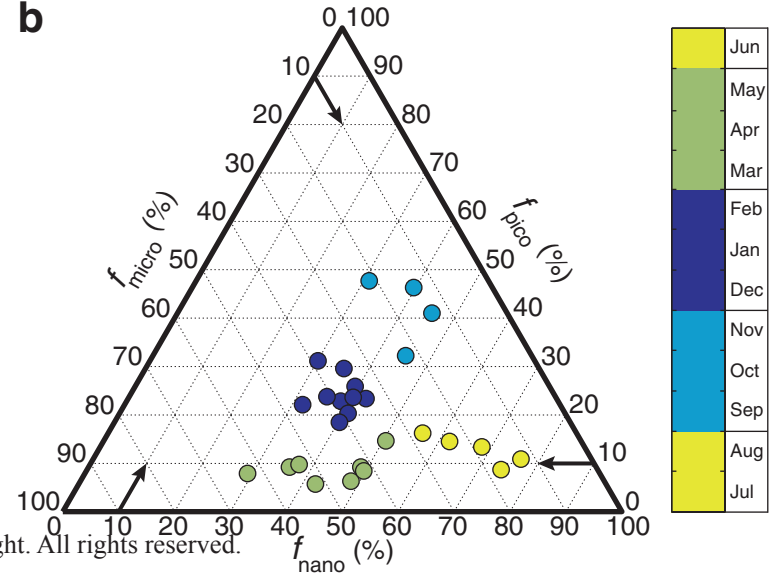

Figure 5.

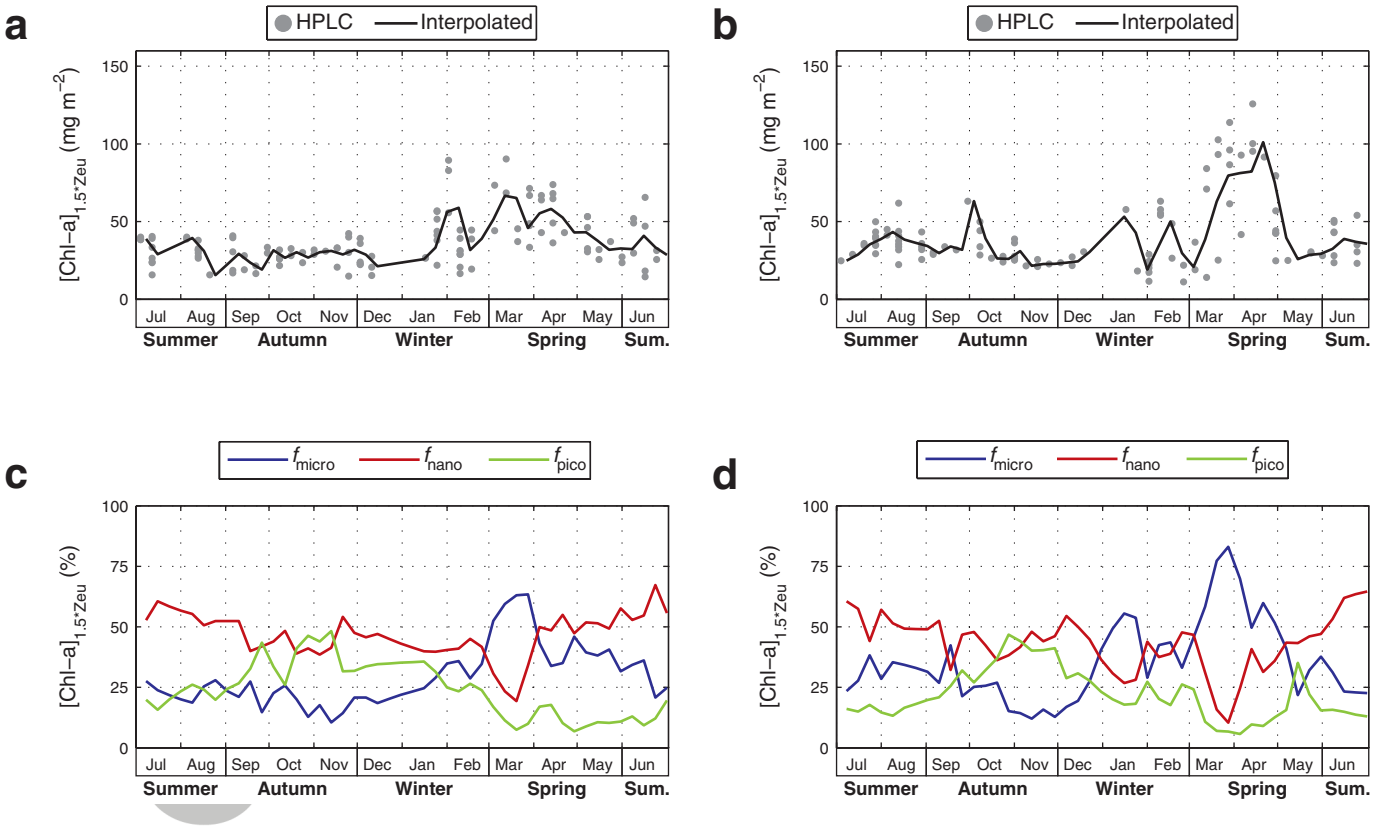

Figure 6.

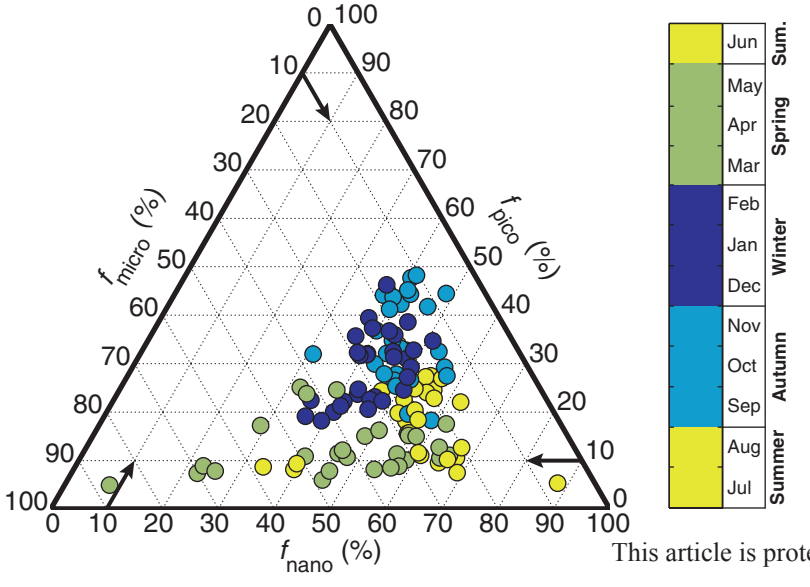

b

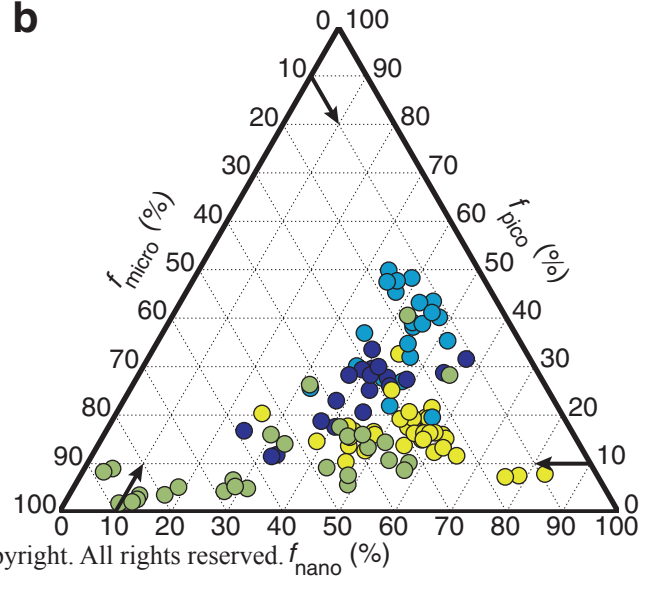

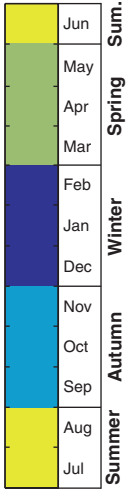

Figure 7.

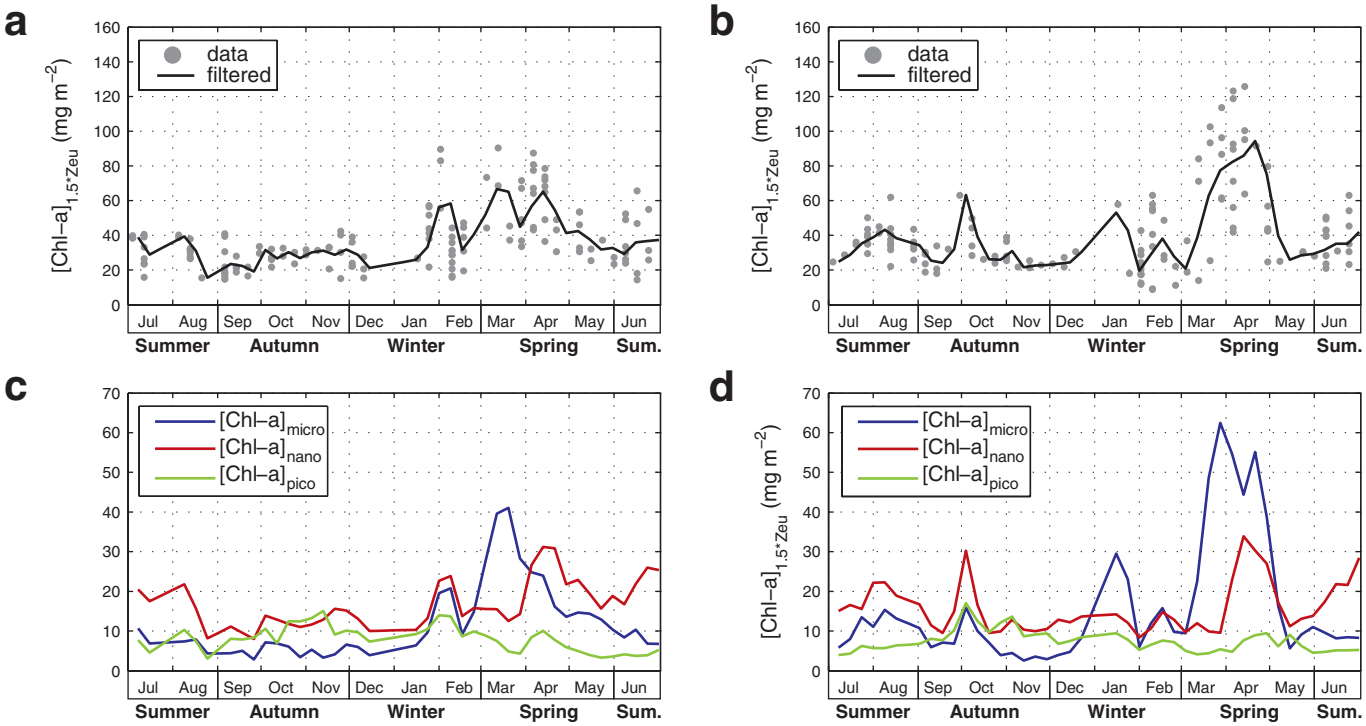

Figure 8.

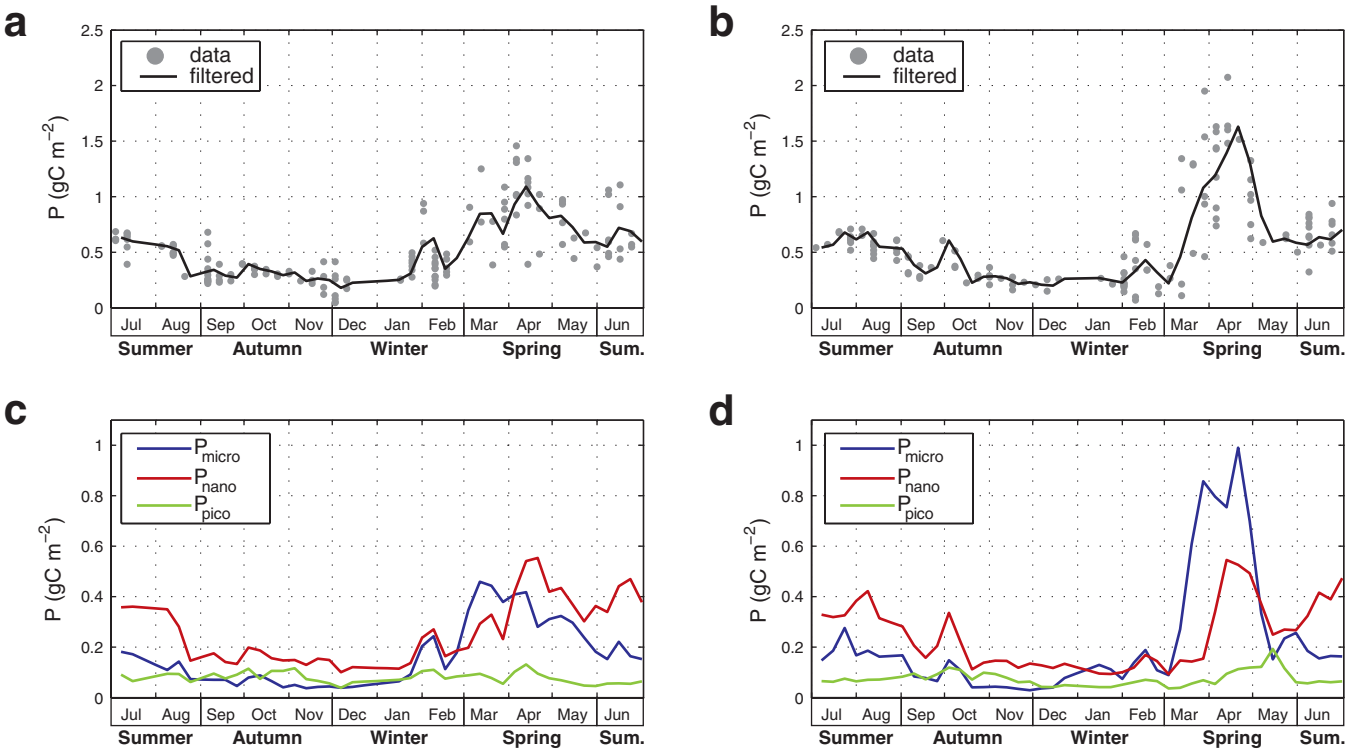

Figure 9.

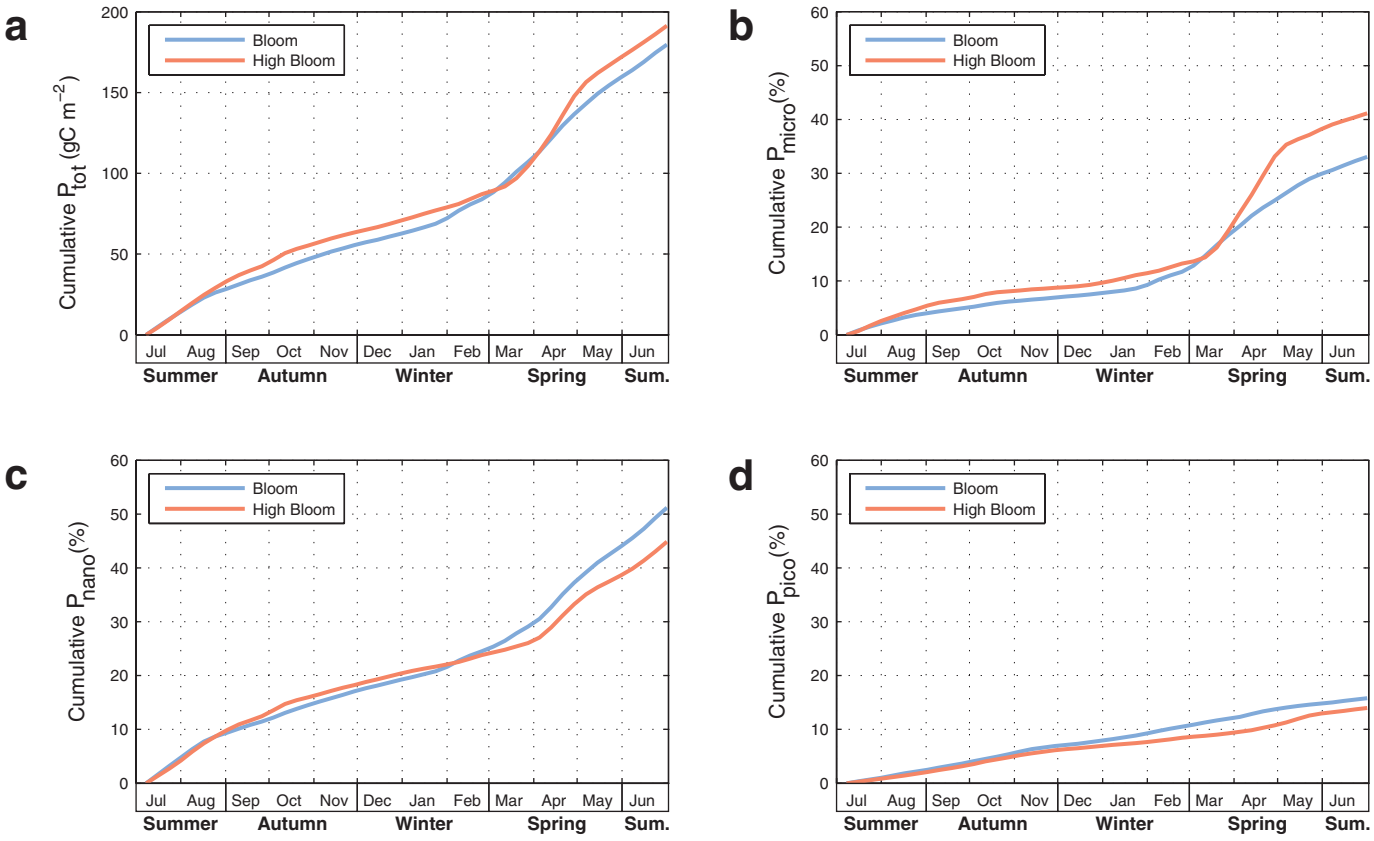

Figure 10.